Some Aspects of the Electron Paramagnetic Resonance Spectroscopy of *d*-Transition Metal Compounds

F. E. Mabbs
Chemistry Department, University of Manchester, Manchester M13 9PL, U.K.

1 Introduction

Electron paramagnetic resonance (EPR) spectroscopy is an extremely powerful probe of the electronic structures of materials with unpaired electrons. There is a variety of EPR techniques, each of which has some particular advantages. The most popular, because of its availability, is continuous wave (CW) EPR spectropscopy.[1,2] In this technique the microwave radiation, used to induce transitions, is applied to the sample continuously. A fixed frequency is used, although different fixed frequencies may be used for specific reasons. When the unpaired electrons are mainly associated with the metal centres CWEPR is the preferred technique. Although CWEPR can give information when the unpaired electrons are delocalized onto surrounding atoms which have non-zero nuclear spin, it has some serious limitations which will be discussed later. These limitations can often be overcome by the use of other methods such as multiple resonance[3] or pulsed techniques.[4] With the availability of commercial instrumentation, there is an increasing use of electron nuclear double resonance (ENDOR) and electron spin echo envelope modulation (ESEEM) spectroscopies. In essence these two techniques record the NMR spectra of (highly) paramagnetic materials.

With respect to *d*-transition metal ions, EPR spectroscopy is widely used to study coordination and organometallic complexes, and metal ion centres in biological materials and in catalysts. The various EPR techniques can be applied at a number of different levels of sophistication; from merely detecting the presence of unpaired electrons, through identifying atoms associated with those unpaired electrons, to detailed descriptions of electronic structures. At whatever level is being considered, it is important that the user realises both the potential and the limitations of the particular technique. Incorrect or over-interpretation should certainly be avoided. Equally, so should under-interpretation, when with some extra effort, more information can be reliably abstracted from the experimental spectra.

Frank Mabbs is a graduate (B.Sc./Ph.D./D.Sc.) of University College, London. His postgraduate research (1957—60), supervised by the now Professor The Lord Lewis, Kt., F.R.S., concerned the magnetic properties of transition metal complexes. After three years as a Technical Officer with British Titan Products at Billingham he moved to the University of Manchester as a NATO Research Fellow, and was subsequently appointed to a Lectureship. He is currently a Senior Lecturer in Inorganic Chemistry. His research interests are in the broad area of the coordination chemistry of d transition metals, and the structures, reactivities and spectroscopic properties (especially EPR) of coordination compounds.

This review will deal with both the commonly and not so commonly occurring interactions which have an effect on experimental EPR spectra. Because the subject area is vast, only cases where an individual metal ion has one unpaired electron will be dealt with. Special attention will be given to CWEPR, since this is most widely used. However, the circumstances under which it will be either profitable, or indeed essential, to use other EPR techniques will be discussed more briefly.

The discussion will be divided into three areas: (1) dilute mononuclear paramagnets, (2) the effects of surrounding paramagnets, and (3) ligand atoms with non-zero nuclear spin.

2 Diluted Monomeric Paramagnets

The main interactions which will be considered as contributing to the EPR spectra are (i) the electronic Zeeman effect and (ii) that between the electron and the metal nuclear spin. For some systems it may also be necessary to include the metal nuclear Zeeman and quadrupole interactions. For any one paramagnet the electronic Zeeman interaction is expressed *via* the *g*-tensor.[5a] There are three mutually orthogonal principal values of *g*. The deviation of these *g*-values from the free electron value of 2.0023 carries information concerning the orbital angular momentum of the electron, *i.e.* information concerning the electronic structure. The interaction between the electron spin and the metal nuclear spin (the metal hyperfine interaction, usually denoted by *A*) is expressed *via* the *A*-tensor.[5b] This is also characterized by three mutually orthogonal principal values. As will be shown in the next section, the directions of the three principle values of *g* and of *A* need not coincide. Their coincidence, or otherwise, is in part determined by the point symmetry at the metal ion.

2.1 The Effects of Point Symmetry

In this context it is important to make the distinction between point symmetry and the more commonly used descriptions of the shapes of complexes. For example, we may have two complexes MA_4 and MA_2B_2 where the ligand atoms are at the corners of a square plane. The common description of both of these complexes would be square planar. However, MA_4 would have D_{4h} point symmetry whereas MA_2B_2 would have either C_{2v} or D_{2h} point symmetry for *cis* and *trans* arrangements, respectively.

The point symmetry at the metal determines whether or not any of the principal *values* of *g* or of *A* are *required* to be equal to each other. Also it determines whether or not any of the principal *axes* of *g* and *A* are *required* to be coincident. These criteria are summarized in Table 1, along with the accepted nomenclature for EPR behaviour and their associated point symmetries. The importance of these relationships is that each type of EPR behaviour is associated with a restricted number of point symmetries. This in turn places constraints upon the geometrical structures of the paramagnet. For example, if we can experimentally demonstrate that a paramagnet really has, say rhombic EPR symmetry, then the associated geometry must belong to one of the point groups D_{2h}, C_{2v}, or D_2. It would be incorrect to assign a structure which belongs to a more symmetric arrangement *e.g.* D_{4h} which is strictly axial.

Table 1 Relationships between g and A tensors, EPR symmetry and the point symmetry of paramagnets

EPR Symmetry	g and A Tensors	Coincidence of Tensor Axes	Molecular Point Symmetry
Isotropic	$g_{xx} = g_{yy} = g_{zz}$ $A_{xx} = A_{yy} = A_{zz}$	All coincident	O_h, T_d, O, T_h, T
Axial	$g_{xx} = g_{yy} \neq g$ $A_{xx} = A_{yy} \neq A$	All coincident	D_{4h}, C_{4v}, D_4, D_{2d}, D_{6h}, C_{6v}, D_6, D_{3h}, D_{3d}, C_{3v}, D_3
Rhombic	$g_{xx} \neq g_{yy} \neq g_{zz}$ $A_{xx} \neq A_{yy} \neq A_{zz}$	All coincident	D_{2h}, C_{2v}, D_2
Monoclinic	$g_{xx} \neq g_{yy} \neq g_{zz}$ $A_{xx} \neq A_{yy} \neq A_{zz}$	One axis of g and A coincident	C_{2h}, C_s, C_2
Triclinic	$g_{xx} \neq g_{yy} \neq g_{zz}$ $A_{xx} \neq A_{yy} \neq A_{zz}$	Complete non-coincidence	C_1, C_i
Axial non-collinear	$g_{xx} = g_{yy} \neq g_{zz}$ $A_{xx} = A_{yy} \neq A_{zz}$	Only g_{zz} and A_{zz} coincident	C_3, S_6, C_4, S_4 C_{4h}, C_6, C_{3h}, C_{6h}

2.2 The Experimental Determination of EPR Symmetry

The previous section has set out the theoretical relationships between EPR symmetry and point symmetry For a system of unknown structure, if the EPR symmetry can be determined we have invaluable structural information since the paramagnetic can only belong to a restricted range of point symmetries The problem is a practical one of how to obtain reliably the above type of information As in all spectroscopic techniques there is often a lack of uniqueness in the interpretation of the experimental data This may arise either from the inadequacies of the data or from different combinations of interactions leading to the same spectrum With this in mind the next two sections explore the usefulness, and the limitations, of experimental CWEPR spectra

2 2 1 Spectra from Powders or Frozen Solutions

These types of spectra are the ones most commonly encountered when investigating materials of unknown structure In this article the term powder spectrum will be used to cover spectra from either powders or frozen solutions For these types of measurement to be useful three essential criteria must be satisfied

(i) There must be no magnetic interactions between the paramagnets, the effects of such interactions are discussed in Section 3 Since such interactions usually arise from the close proximity of the paramagnets, this means that they must be in low concentration, *i e* magnetically dilute The dilution *must* be at the *molecular* level Thus for powders, no matter how finely they are powdered, *mechanical mixing* is unsatisfactory

(ii) The methods for interpreting the spectra require there to be completely random orientations of the paramagnets in the sample Thus the diluted solids must be powdered sufficiently so that there are no preferential orientations of small crystallites Similarly solutions must be frozen to form a glass, thereby avoiding the formation of crystallites

(iii) The randomness of the paramagnets in the sample should always be checked by repeating the spectrum after the sample has been turned through an angle, for example of about 20° If the two spectra are not *identical* then the paramagnets in the sample are not completely randomly oriented

The determination of the EPR symmetry from spectra is the next important step This step is often inadequately performed, leading to possible incorrect assignments of the EPR symmetry and hence the electronic and geometric structures With the aid of some selected samples, both the power and the limitations of methods of determining the EPR symmetry from powder spectra will be shown

The simplest situations arise when there are no hyperfine interactions In these cases it is usually a question of determining whether or not the paramagnet has axial or rhombic g values

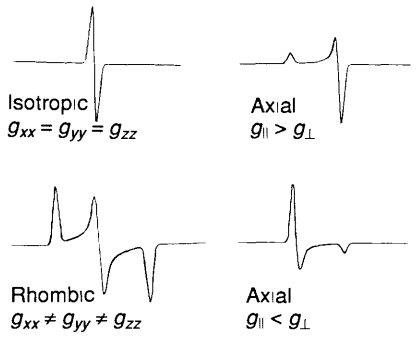

Figure 1 Idealized EPR patterns for different EPR symmetries considering g anisotropy only For axial EPR symmetry $g = g_z$ and $g_{\perp} = g_{xx} = g_{yy}$

When the resonances for the principal g values of the paramagnet are sufficiently well separated compared to the linewidths of the resonances, then this presents no problems This situation is represented by the simulated spectra in Figure 1 However, if the anisotropy, in for example two of the g values, is such that at a particular microwave frequency the resonance magnetic fields are not well separated compared with the linewidths then the spectra could be (mis-)assigned to an EPR symmetry which is too high An example of this is in Figure 2a, where the spectrum at X-band could easily be mistakenly assigned to axial EPR symmetry When spectra appear to correspond to axial EPR symmetry at X-band it is important to do at least one, but preferably both of the following

(i) a full simulation of the spectrum, including linewidths and lineshapes as variables, should be performed,

(ii) the spectrum should be obtained at a higher microwave frequency

For the particular example shown in Figure 2, the Q-band spectrum clearly demonstrates that the paramagnet concerned has rhombic g values, see Figure 2b Note that when only the g value anistropy is the experimental observable, there is a much greater choice of associated point symmetries For example for rhombic g values the point symmetry of the molecule could be any of those corresponding to the EPR symmetries rhombic, monoclinic, or triclinic I will return to the example used in Figure 2 a little later to show how an analysis of *both* the g and A tensors can narrow the choice of point symmetries

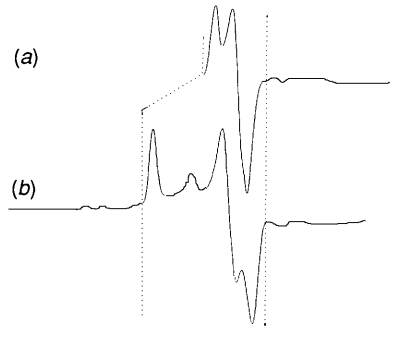

Figure 2 A comparison of (a) the X- and (b) the Q-band spectra of the $I = 0$ isotopes of molybdenum (the parts of the spectra within the dashed lines) for $[LMoOCl_2]$, where L = hydrotris (3,5-dimethylpyrazolyl)borato

The presence of a metal hyperfine interaction can be extremely useful in two particular ways It provides (i) an additional means of detecting anisotropy in the system, and (ii) the possibility of determining the coincidence or otherwise of the principal axes of the g and A tensors Let us first consider a typical visual difference between the spectra of an axial and a rhombic paramagnet Figure 3 shows X-band spectra for two vanadium(IV) species, one of which has axial and one which has

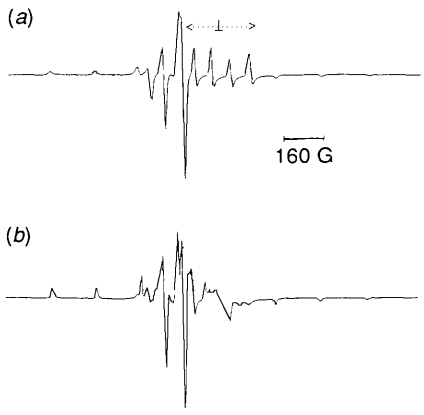

Figure 3 A comparison of the experimental powder EPR spectra (a) an axial system represented by $[VO(imid)_4Cl]^+$ in CH_3CN/imid, where imid = 1 vinylimidazole, and (b) a rhombic system represented by $[VO(Mequin)_2]$, where Mequin = 2-methylquinolin-8-olato

rhombic or lower, EPR symmetry In these cases the major differences between the spectra are the splittings, which occur in the rhombic spectrum, of those features corresponding to those labelled '⊥' in the axial spectrum

An example which represents a severe test of the combined use of more than one microwave frequency and of spectrum simulation is provided by $H_2[V(R,R\text{-HIDPA})_2]$ diluted in the corresponding zirconium compound, see Figures 4 and 5 An initial look at *both* the X- and Q-band spectra suggests that the system has axial EPR symmetry, since the features in the region of the spectra associated with the x and y directories (equivalent to those labelled '⊥' in Figure 3) of the system are not split However, all attempts to simulate both the X- and Q-band spectra, based on axial EPR symmetry, are not entirely satisfactory, compare Figures 4a and 4b, and Figures 5a and 5b The introduction of a small anisotropy into both g_{xx}, g_{yy} and A_{xx}, A_{yy}, produces an improved simulation at *both* frequencies, see Figures 4c and 5c Although the rhombicity is small it is consistent with the known structure of the compound [6] From the crystallography, the highest possible point symmetry at the vanadium is C_2

The following two examples also provide additional reasons for performing detailed spectrum simulations The features in a powder spectrum arise from turning points in the angular variation of the resonance fields within the system Turning points in $S = 1/2$ systems occur when the magnetic field is parallel to the principal axes of the g and A tensors These features are marked X, Y, or Z on the simulated spectra in Figures 6 and 7 However, for some combinations of the principal g and A values there may be turning points at other orientations, *i e* 'off-axis' turning points This is illustrated in Figure 6, giving rise to what is termed an 'overshoot' feature Such features are often observed in the X-band spectra of copper(II) species In Figure 7 there are also 'off-axis' turning points, but these now occur at the low field end of the spectrum and can thus be termed 'undershoot' features The features attributed to the 'off-axis' turning points can have greater amplitudes in the powder spectra than some of those which belong to the principal directions At first sight it would be tempting to assign the 'overshoot' or 'undershoot' features to the principal directions Such an assignment would either lead to incorrect principal values of g and A, if the spectra were interpreted by simply 'reading off' magnetic field positions, or to an inability to interpret all the features in the spectra

We now turn our attention to the much more difficult task of trying to determine whether or not the g and A tensors are coincident It is important that any putative non-coincidence should be confirmed by spectrum simulation Are there any guidelines with respect to the form of a powder spectrum which might suggest the presence of non-coincidence? The answer is

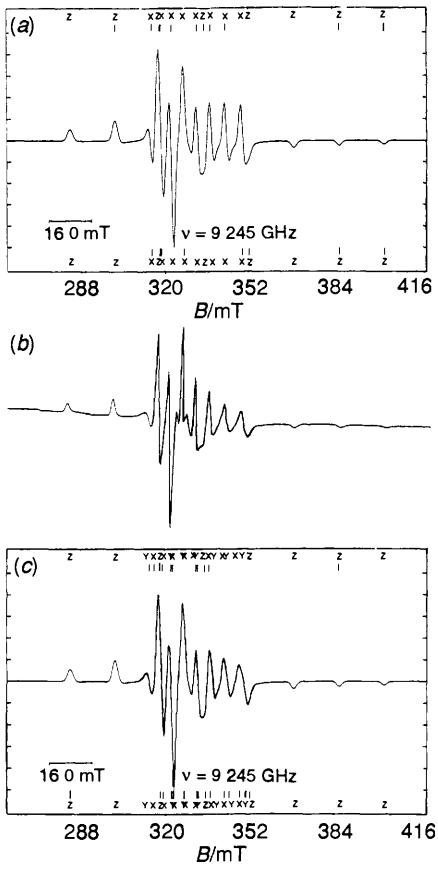

Figure 4 A comparison of the experimental and simulated X-band powder EPR spectra of $H_2[V(R,R\text{-HIDPA})_2]$ diluted in the zirconium analogue where HIDPA = hydroxyiminodipropionate (a) Simulated assuming axial EPR symmetry and $g = 1\,9195$, $g_\perp = 1\,9839$ $A = 17\,15$ mT, $A_\perp = 4\,9$ mT, ΔB(p–p) = 2 0 mT, ΔB(p–p)$_\perp$ = 1 6 mT, (b) experimental, (c) simulated assuming rhombic EPR symmetry and $g = 1\,9195$, $g_{xx} = 1\,9848$, $g_{yy} = 1\,9829$, $A = 17\,15$ mT, $A_{xx} = 4\,6$ mT, $A_{yy} = 5\,2$ mT, ΔB(p–p) = 2 0 mT, ΔB(p–p)$_{xx}$ = $\Delta B(p\text{–}p)_{yy}$ = 1 6 mT A Gaussian lineshape function was used in the simulations

yes, under some circumstances The first indication of non-coincidence is usually that there appear to be either too many features in the spectrum, or that there are features in the wrong place compared to those predicted from simple considerations with the g and A tensor axes coincident Examples of this are in Figures 8 and 9 In these two cases extrapolating the positions of the hyperfine features starting from either end of the spectrum produces, either some features which are unaccounted for (see Figure 8), or predicted positions where no features appear in the spectrum (see Figure 9) Some caution is advised with this approach, as we must be sure that any extra features are not due to impurities, or that failure of the extrapolated features to match those in the spectrum is not due to second-order effects An additional indication that there is non-coincidence is the inability to simulate spectra assuming coincidence However, this is a negative reason, and the lack of success in the simulation could be due to other reasons Also, if this lack of success were taken as a starting point for trying to discover non-coincidence, relying on further spectrum simulation could be very time consuming

The considerations in the previous paragraph require suitable simulation programs, and also considerable effort However, if the information concerning non-coincidence of the g and A tensor axes can be obtained, it restricts further the point groups to which the paramagnet can belong For example, we have found this approach particularly useful in the series of oxomolybdenum(v) compounds of formula $[LMoO(X_2)]$, where L = hydrotris(3,5-dimethylpyrazolyl)borato When the donor

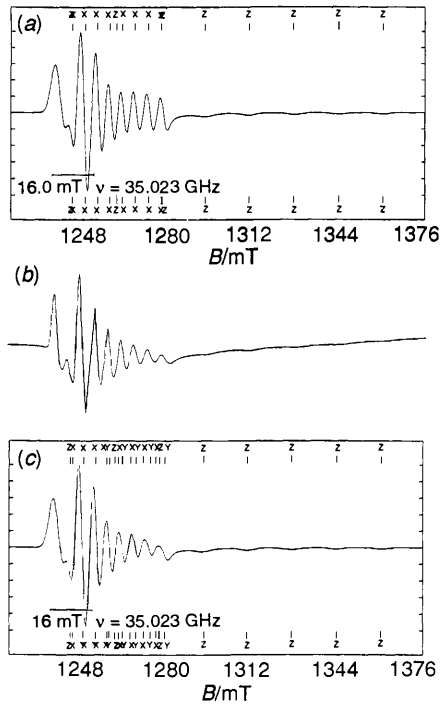

Figure 5 A comparison of the experimental and simulated Q-band powder EPR spectra of $H_2[V(R,R\text{-HIDPA})_2]$ diluted in the zirconium analogue, where HIDPA = hydroxyiminodipropionate. (a) Simulated assuming axial EPR symmetry and $g_{\parallel} = 1.9195$, $g_{\perp} = 1.9839$, $A = 17.15$ mT, $A_{\perp} = 4.9$ mT, $\Delta B(\text{p–p})_{\parallel} = 5.4$ mT, $\Delta B(\text{p–p})_{\perp} = 2.4$ mT, (b) experimental, (c) simulated assuming rhombic EPR symmetry and $g_{zz} = 1.9195$, $g_{xx} = 1.9848$, $g_{yy} = 1.9829$, $A_{zz} = 17.15$ mT, $A_{xx} = 4.6$ mT, $A_{yy} = 5.2$ mT, $\Delta B(\text{p–p})_{zz} = 5.4$ mT, $\Delta B(\text{p–p})_{xx} = \Delta B(\text{p–p})_{yy} = 2.4$ mT. A Gaussian lineshape function was used in the simulations.

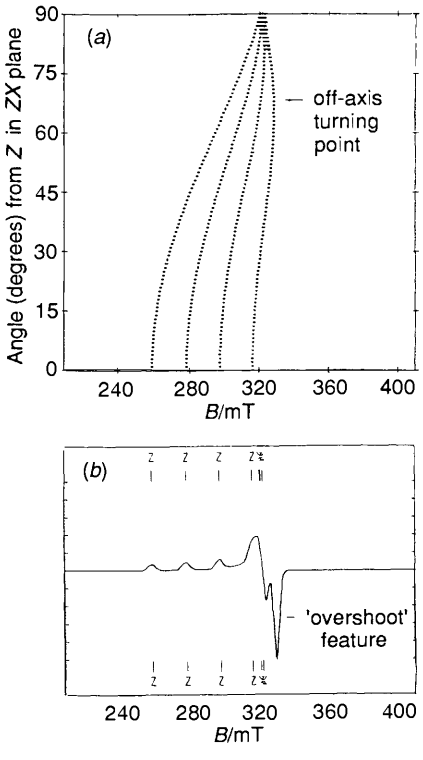

Figure 6 Simulated powder spectrum showing the 'overshoot' feature in an axial paramagnet with $S = 1/2$, $I = 3/2$, $g_{\parallel} = 2.300$, $g_{\perp} = 2.050$, $K_{\parallel}19.0$ mT, $K_{\perp} = 1.0$ mT, isotropic $\Delta B(\text{p–p}) = 4.0$ mT, $\nu = 9.250$ GHz. (a) Variation of the resonance fields with θ, (b) the powder spectrum. Resonance fields at the axes are marked Z for the parallel direction and X for the perpendicular direction. Any features not marked in this way belong to 'off-axis' turning points.

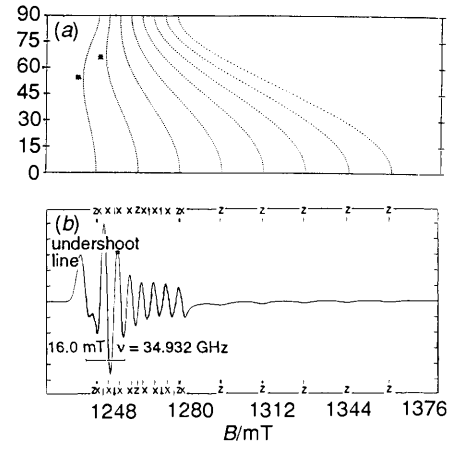

Figure 7 Simulation of an axial powder spectrum of a vanadium(IV) species showing the 'undershoot' features. (a) The angular variation of the resonance field with θ('off-axis' turning points are denoted by *). Simulation parameters were: $g_{\parallel} = 1.9195$, $g_{\perp} = 1.9839$, A 17.15 mT, $A_{\perp} = 4.9$ mT, $\Delta B(\text{p–p})_{\parallel} = 5.2$ mT, $\Delta B(\text{p–p})_{\perp} = 2.4$ mT, Gaussian lineshape. Resonance fields at the axes are marked Z for the parallel direction and X for the perpendicular direction. Any features not marked in this way belong to 'off-axis' turning points.

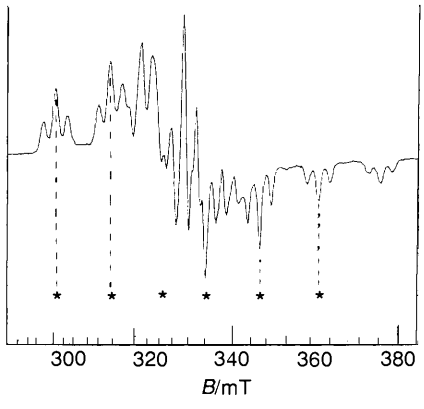

Figure 8 X-Band frozen solution spectrum of $[(\eta^5\text{-}6\text{-}exo\text{-}PhC_6H_6)Mn(CO)(dppe)]^+$ in $CH_2Cl_2/ClCH_2CH_2Cl$, where dppe = bis(diphenylphosphino)ethane. The asterisks indicate the expected positions of the central component of the 1:2:1 triplets extrapolated from the position of the lowest field feature.

The experimental spectrum was kindly supplied by Dr. P. H. Rieger. See also R. D. Pike, A. L. Rieger, and P. H. Rieger, *J. Chem. Soc., Faraday Trans., 1*, 1989, **85**, 3913.

atoms represented by X_2 are either monodentate ligands or bidentate ligands with a symmetric donor set, the powder spectra are interpretable in terms of monoclinic EPR symmetry.[7] This indicates that these molecules have C_{2h}, C_s, or C_2 point symmetry. For C_s point symmetry, the only symmetry element is a mirror plane. Where *X*-ray structures are available, the presence of a mirror plane, or very nearly mirror symmetry, is found for those compounds where powder EPR spectra indicate monoclinic EPR symmetry.

In case the discussion so far gives the impression that powder EPR spectra will always provide detailed information on point symmetry, a word of caution must be injected. If the angle of non-coincidence is small, say $< 10°$, then it may be difficult to detect from powder spectra. Experience has shown that the simulated spectra are often insensitive to such small angles of non-coincidence, particularly when the anistropy in both the g and A tensor elements being rotated is small. Sometimes the lower the experimental microwave frequency the easier it is to detect the presence of non-coincidence.

If we wish to use the information from powder spectra to discuss the details of electronic structure then there are some

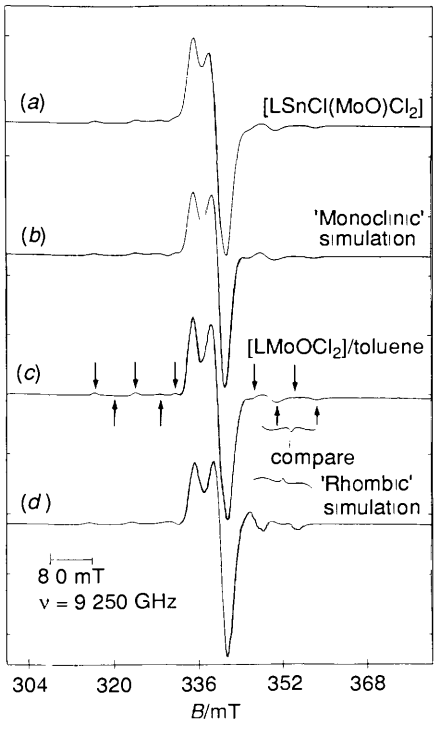

Figure 9 Powder type spectra at 77 K of $[LMoOCl_2]$, where L = hydrotris(3,5-dimethylpyrazolyl)borato, dissolved in (a) $[LSnCl_3]$ and (c) toluene The arrows in (c) indicate the extrapolated positions of the hyperfine features starting from either end of the spectrum (b) and (d) are simulations using the parameters $g_{11} = 1\ 971$, $g_{22} = 1\ 941$, $g_{33} = 1\ 934$, $A_{11} = 71\ 4 \times 10^{-4}$ cm $^{-1}$, $A_{22} = 18\ 1 \times 10^{-4}$ cm^{-1}, $A_{33} = 38\ 1 \times 10^{-4}$ cm^{-1}, $\Delta B(\text{p-p})_{11} = 3\ 0$ mT, $\Delta B(\text{p-p})_{22} = \Delta B(\text{p p})_{33} = 2\ 5$ mT, and (b) the angle of non-coincidence between g_{11}/A_{11} and g_{33}/A_{33} equal to 33°, (d) complete coincidence of the g and A tensors A Gaussian lineshape function was used in the simulations

additional considerations At best the powder EPR spectra give the *values* of the g and A tensors and their relationship to each other However, we have no *direct* means of assigning a given tensor element to any particular direction in the paramagnet This is especially true in low symmetry systems, where it cannot be assumed that the principal axes of the tensors will correspond to metal–ligand directions If we wish to discuss the electronic structure in detail then it is essential not only to know the geometric structure of the paramagnet, but also to know the orientation of the tensors with respect to the atomic framework A detailed single crystal study, on crystals for which the *X*-ray crystal structure is known, is now required

2 2 2 *Single Crystal Spectra*

Single crystal measurements are often performed in three mutually orthogonal planes AB, BC, AC, with respect to the orthogonal axes A, B, and C It is convenient, but not essential for A, B, and C to be the orthogonalized crystallographic axes The electronic Zeeman effect and the hyperfine interaction are expressed in the *measuring* axis system *via* the symmetric tensors

$$\begin{array}{c} \\ A \\ B \\ C \end{array}\begin{array}{c} \begin{array}{ccc} A & B & C \end{array} \\ \begin{pmatrix} (g_{AA})^2 & (g_{AB})^2 & (g_{AC})^2 \\ (g_{BA})^2 & (g_{BB})^2 & (g_{BC})^2 \\ (g_{CA})^2 & (g_{CB})^2 & (g_{CC})^2 \end{pmatrix} \end{array} \quad \text{and} \quad \begin{array}{c} \\ A \\ B \\ C \end{array}\begin{array}{c} \begin{array}{ccc} A & B & C \end{array} \\ \begin{pmatrix} (K^2g^2)_{AA} & (K^2g^2)_{AB} & (K^2g^2)_{AC} \\ (K^2g^2)_{BA} & (K^2g^2)_{BB} & (K^2g^2)_{BC} \\ (K^2g^2)_{CA} & (K^2g^2)_{CB} & (K^2g^2)_{CC} \end{pmatrix} \end{array}$$

where $(g_{ij})^2 = (g_{ji})^2$ and $(K^2g^2)_{ij} = (K^2g^2)_{ji}$ for $i \neq j$

In most cases it is possible to obtain only the magnitudes, but not the signs, of the above tensor elements [8] The usual reason for this is that there may be magnetically inequivalent, but chemically identical, paramagnets in the crystal This creates a problem of relating the signals to specific paramagnets in the different measuring planes in the crystal The same situation arises if the crystal has to be remounted or if more than one crystal has to be used These problems are equivalent to uncertainties in the positive or negative senses of rotation with respect to the A, B, C measuring axes The result is that we do not know the relative signs of the off-diagonal elements within either of the tensors, but the relative sign of equivalent $(g_{ij})^2$ and $(K^2g^2)_{ij}$ is determined Thus for this type of measurement, *a priori* there are eight alternative solutions for *each* of the tensors These alternatives correspond to all possible sign combinations of the off-diagonal elements The inter-connection between these alternatives is shown in Scheme 1

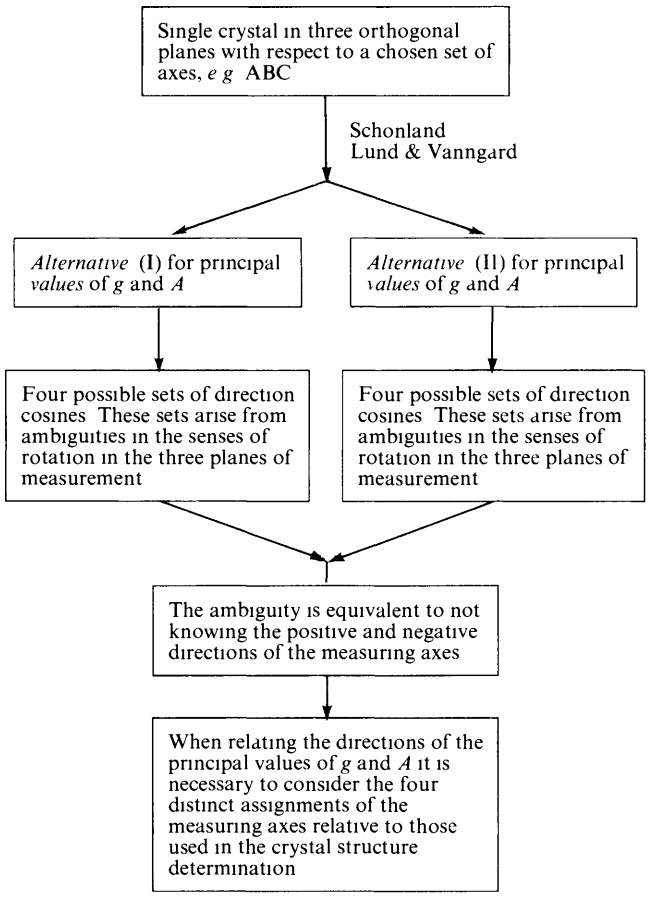

Scheme 1

How can the correct alternative be found? The ambiguities in the signs of the off-diagonal elements can be removed by taking measurements in a fourth plane in the crystal [8 9] The choice of this plane, with respect to the original ABC axes, will depend upon the alternatives to be distinguished and upon the ability to orient accurately the crystal in the chosen plane Measurements such as these may resolve the ambiguities in both the values and orientations of the tensors with respect to the measuring axes [9] If for any reason a suitable fourth plane cannot be measured, a choice between the two sets of *values* can often be made *via* a comparison of the experimental powder spectrum and simulations based on the two alternative sets of values An example of this is illustrated for $[LMo\{V\}O(Et_2dtc)]$, where Et_2dtc = *N N*-diethyldithiocarbamate The alternative values are given in Table 2 and the comparison between the experimental and simulated powder spectra is in Figure 10 In this particular example this comparison rules out *Alternative I* However, with this procedure we are still left with deciding which of the four alternative *orientations* of the tensors with respect to the measuring axes is the correct one This is equivalent to not knowing the positive and negative senses of the measurement axes with respect to the crystallographic axes

Table 2 The principal values, direction cosines, and angles between the g and A tensors for [LMo{V}O(Et_2dtc)] (The axes for measurement were assigned as a b c^*)

Alternative I

	a	b	c^*
g_{11} = 1 958	0 9388	0 3320	− 0 0918
g_{22} = 1 980	0 1678	− 0 6735	− 0 7199
g_{33} = 1 988	0 3009	− 0 6604	0 6880
A_{11} = 150 3	− 0 9220	− 0 3555	0 1533
$\lvert A_{22}\rvert$ = 76 6	− 0 1407	0 6767	0 7227
$\lvert A_{33}\rvert$ = 2 2	0 3607	− 0 6448	0 6739

Angles (°) between the g and A tensors

	A_{11}	A_{22}	A_{33}
g_{11}	176 1	88 7	86 4
g_{22}	91 5	178 4	89 5
g_{33}	86 4	89 5	3 6

Alternative II

	a	b	c^*
g_{11} = 1 958	− 0 9219	− 0 3508	0 1646
g_{22} = 1 983	0 3636	− 0 6364	0 6803
g_{33} = 1 986	− 0 1339	0 6870	0 7143
$\lvert A_{11}\rvert$ = 151 9	− 0 9032	− 0 3742	0 2101
$\lvert A_{22}\rvert$ = 53 0	0 4109	− 0 6126	0 6752
$\lvert A_{33}\rvert$ = 51 0	0 1239	− 0 6962	0 7071

Angles (°) between the g and A tensors

	A_{11}	A_{22}	A_{33}
g_{11}	3 1	93 0	89 2
g_{22}	87 0	3 1	89 6
g_{33}	89 2	89 6	179 1

The A values are in units of 10^{-4} cm^{-1} Estimates errors ± 0 001 for g values and ± 0 5 × 10^{-4} cm^{-1} for A values

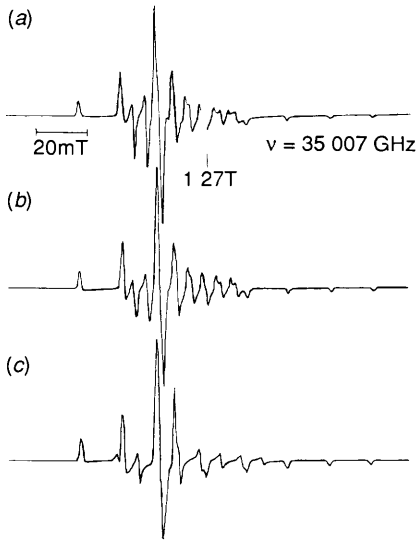

Figure 10 Comparison of (a) the room temperature spectrum of a diluted powder of [LMo{V}O(Et_2dtc)] with simulations for (b) *Alternative II*, and (c) *Alternative I* in Table 2 In addition to the parameters in Table 2 an isotropic ΔB(p–p) = 1 0 mT, and a Gaussian lineshape function, were used

The next stage of the analysis from either of the above approaches is to relate the experimental orientations of the tensor axes to the atomic framework of the paramagnet If we have an unambiguous orientation of the tensors with respect to the measuring ABC axes then all that remains is to transform these orientations into the crystallographic framework The directions of the tensors can then be compared with metal–ligand directions calculated from the crystallography To do this it is essential that the relative orientations of the positive ABC measuring axes and the positive crystallographic axes are known *unambiguously* If the experiment has left us with four alternative sets of orientations then the choice of the correct one is more difficult This is because in general we cannot assume that the tensor axes will coincide with any particular orientations with respect to the atomic framework of the paramagnet The reasons for the alternative answers were the ambiguities in the senses of rotation in the measurement framework This is equivalent to not knowing the positive senses of the measurement axes with respect to the positive directions of the crystallographic axes

When the four alternative sets of orientations have been transformed into the crystallographic framework, extra criteria are required in order to choose the appropriate orientation of the tensor axes with respect to the atomic framework For example, in the molecule [LVO(Et_2dtc)], the crystal structure shows that, although it is not a crystallographic requirement, there is an approximate mirror plane in the molecule, *i e* the molecule approximates to C_S point symmetry Therefore the alternative having one g and one A tensor axis nearly mutually coincident and perpendicular to the approximate mirror plane in the molecule was the one chosen [10]

3 The Effects of Surrounding Paramagnets

This topic could be wide ranging but, because of restrictions on space, the discussion will be confined to magnetic interactions between paramagnetic centres (i) within isolated dimers and (ii) in undiluted solids The mechanisms whereby the magnetic interactions occur will not be discussed

3.1 Isolated Dimers

The important interactions within a dimer which determine the form of the EPR spectrum are usually the electronic Zeeman effect, the metal hyperfine interaction, electron–electron dipole interactions, and magnetic exchange The particular form of the spectrum will depend upon the relative magnitudes of these interactions The following discussion will be restricted to dimers composed of chemically equivalent metal centres

3 1 1 Magnetic Exchange and Metal Hyperfine Interactions in Dimers in Fluid Solution

The case of an isotropic system (or an anisotropic system tumbling rapidly in solution) will be treated for the effects of isotropic magnetic exchange, metal hyperfine interaction, and magnetic field These interactions are expressed *via* the spin-Hamiltonian (1)

$$\boldsymbol{H} = g\beta_e B(\hat{S}_Z + \hat{S}_{Z_2}) + A(\hat{S}_1 \hat{I}_1 + \hat{S}_2 \hat{I}_2) + JS_1 S_2 \qquad (1)$$

The exchange interaction gives rise to an electronic spin singlet and an electronic spin triplet The spin singlet ($S = 0$) is lowest for antiferromagnetism whilst the spin triplet ($S = 1$) is lowest for ferromagnetism The spin functions required for the dimer must specifically include the nuclear spins of the two centres, *i e* $|S,M_S,I_1,m_I(1),I_2,m_I(2)\rangle$, a total of $(2I_1 + 1)(2I_2 + 1)$ functions

for each electronic spin function In the case of a dimer consisting of two ^{51}V nuclei ($I = 7/2$), an example which will be used shortly, there are a total of 256 functions to consider Obtaining the energies and spin functions exactly by applying (1) would require the diagonalization of a 256 × 256 matrix This is possible with modern computers, but it makes it difficult to produce closed form expressions for the resonance magnetic fields If we assume that a first order calculation will suffice then (1) can be rewritten as

$$\boldsymbol{H} = g\beta_e B(\hat{S}_{Z1} + \hat{S}_{Z2}) + A(\hat{S}_{Z1}\hat{I}_{Z1} + \hat{S}_{Z2}\hat{I}_{Z2}) + J\hat{S}_1 S_2 \quad (2)$$

The problem now reduces to a 4 × 4 matrix for each combination of $m_I(1)$ and $m_I(2)$, and this can be diagonalized algebraically [11] The result is that for each possible combination of $m_I(1)$ and $m_I(2)$ there are four allowed transitions These are summarized in Table 3 Within the approximations above, the resonance fields and their relative intensities are valid whatever the relative values of J and A This type of treatment has been applied to a number of nitroxide biradicals [12] Some simulated spectra for a vanadium(IV) dimer are shown in Figures 11 and 12 When

Table 3 Resonance magnetic fields, resonance type and relative intensities of the allowed transitions

Resonance Field	Resonance Type	Relative Intensities
$B_1 = B_0 + [J + R - A\{m_I(1) + m_I(2)\}]/2g\beta e$	S	$(R - J)/4R$
$B_2 = B_0 + [J - R - A\{m_I(1) + m_I(2)\}]/2g\beta e$	T	$(R + J)/4R$
$B_3 = B_0 - [J + R + A\{m_I(1) + m_I(2)\}]/2g\beta e$	S	$(R - J)/4R$
$B_4 = B_0 - [J - R + A\{m_I(1) + m_I(2)\}]/2g\beta e$	T	$(R + J)/4R$

S resonances and T resonances are those for which the predominant spin functions belong to the spin singlet state and spin triplet states respectively
$R = \{J^2 + A^2(\Delta m)^2\}^{\frac{1}{2}}$ $\Delta m = \{m_I(1) - m_I(2)\}$

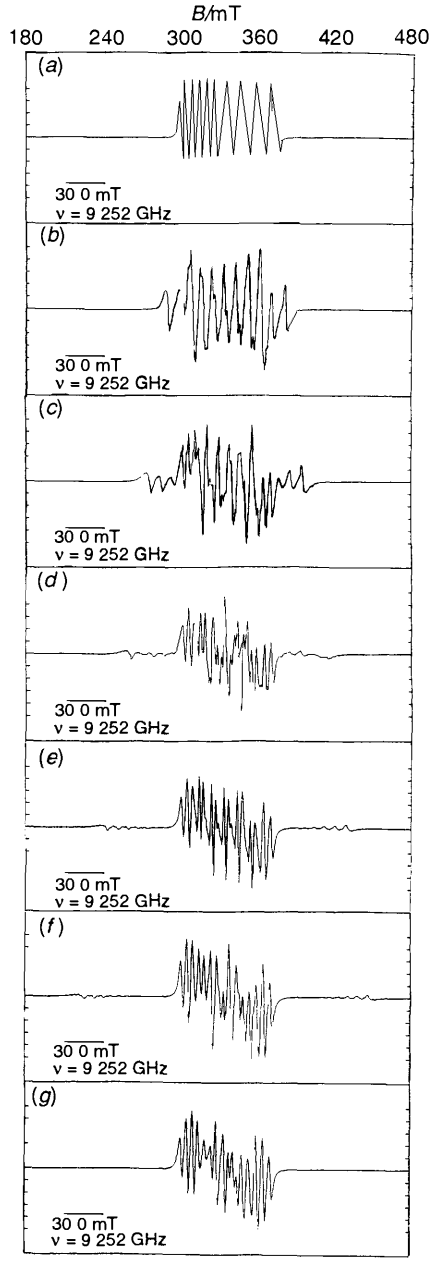

Figure 11 Simulated spectra showing the effect of varying $|J|/|A|$ for a vanadium(IV) dimer The values of $|J|/|A|$ are (a) 0 (b) 2 (c) 4 (d) 6 (e) 8 (f) 10 (g) 18 An M_I independent ΔB(p–p) of 2 1 mT and a Lorentzian lineshape function were used

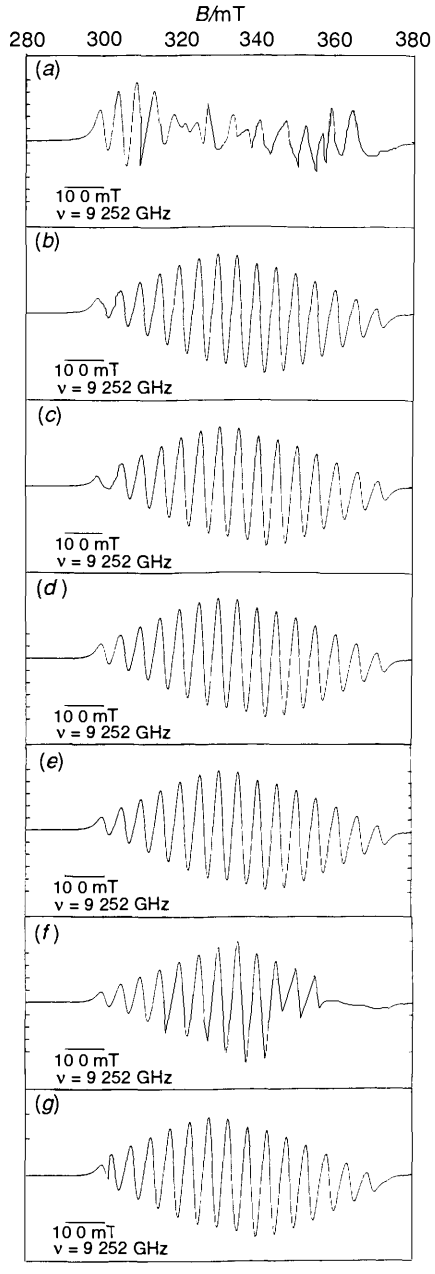

Figure 12 Simulated spectra showing the effect of varying $|J|/A$ for a vanadium(IV) dimer The values of $|J|/|A|$ are (a) 20 (b) 30 (c) 50 (d) 70 (e) 100 (f) 500 (g) 1000 An M_I independent ΔB(p–p) of 2 1 mT and a Lorentzian lineshape function were used

$|J| = 0$, the spectrum is that expected for a monomer and when $|J| \gg |A|$ we obtain the number of lines and the relative intensities which are usually regarded as characteristic of a dimer. In between these limits the predicted form of the spectrum depends upon $|J|/|A|$. When $|J|$ and $|A|$ are comparable weak S resonances are predicted, and they provide[12] a useful way of measuring $|J|$. As $|J|$ becomes larger than $|A|$ the intensities of the S resonances rapidly decrease to zero. The T resonances also show a dependence on $|J|/|A|$, a dependence which persists after the S resonances are too weak to observe. However, eventually the T resonances become insensitive to increasing $|J|/|A|$. In the example shown this occurs for $|J|/|A|$ greater than about 100.

The simulated spectra in Figures 11 and 12 have assumed the same linewidth for all transitions. However, it is well established that linewidths are M_I dependent for anisotropic species which are tumbling,[13] see for example Figure 13. This M_I dependence usually takes the form:

$$\Delta B(\text{p–p}) = a + bM_I + c(M_I)^2 \qquad (3)$$

where ΔB(p–p) is the peak–peak linewidth, and for a dimer $M_I = m_I(1) + m_I(2)$. The imposition of such a linewidth function is to modify the appearance of the spectra in Figures 11 and 12. The most noticeable effect on the simulated spectra is the significant broadening of the features at the extremities of the spectra, particularly at the high field end.

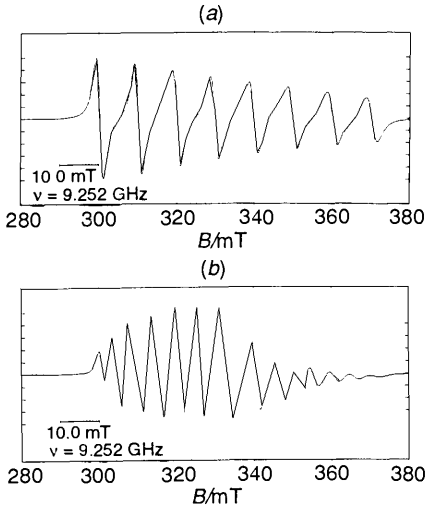

Figure 13 The effect of M_I dependent linewidths on the simulated spectrum of (a) a vanadium(IV) monomer and (b) a vanadium(IV) dimer. The linewidth parameters in equation 3 were $a = 2.20$ mT, $b = 0.2$ mT, $c = 0.01$ mT. A Lorentzian lineshape function was used.

If the exchange interaction fluctuates with time about the static value $|J|$ then there may be additional linewidth effects.[12] These have been observed in some nitroxide biradicals, and they result in an alternation of the amplitudes of the lines in the derivative spectrum.[12] In the limit of very rapid exchange ($J > A$), the expression for the linewidth in the dimer becomes:

$$\Delta B(\text{p–p}) = a + b\{m_I(1) + m_I(2)\}^2 + c\{m_I(1) + m_I(2)\}^2 + d\{m_I(1) - m_I(2)\}^2 \qquad (4)$$

The last term in (4) is the one responsible for the alternation of the amplitudes. The parameter d contains the information concerning both the fluctuation of the exchange about its static value J and the correlation time for the fluctuation.

Unusual relative amplitudes in EPR spectra can also occur for transition metal dimers. Three selected examples which exhibit slightly differing effects are given in Figure 14.

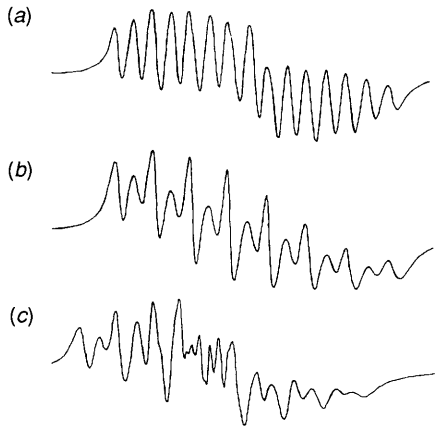

Figure 14 Experimental fluid solution X-band spectra at room temperature of (a) [{LVO(pzh)}(μ-malonato){LVO}], (b) [{LVO(pzh)}$_2$(μ-acetylenedicarboxylato)], (c) [{LVO(pzh)}$_2$(μ-benzene-1,4-dicarboxylato)], where pzh = 3,5-dimethylpyrazole and L = hydrotris(3,5-dimethylpyrazolyl)borato. The scan range on each spectrum is 100 mT.

3.2 Undiluted Solids

For reasons which will become apparent as the discussion progresses, it is often thought that obtaining the EPR spectrum of an undiluted solid is a waste of time. One of the major reasons for this view is the presence of *inhomogeneous* line broadening which occurs as a result of interactions which affect the *energies* of the spin states involved in the EPR transitions. However, adopting a pragmatic view, a preliminary investigation of the spectrum (preferably at more than one microwave frequency) is always worthwhile. Occasionally there are interesting surprises, and sometimes even unpromising looking spectra can yield information.

For *d* transition metal compounds the most common causes of line broadening in undiluted solids are electron–electron dipolar and exchange interactions. For any given paramagnetic centre the dipole–dipole interaction due to surrounding paramagnets creates a magnetic field at that paramagnet. This is an additional field which is superimposed on the applied magnetic field. In a solid it is unlikely that all the paramagnets in the sample will experience the same additional field, and hence the spectrum is broadened. Electronic exchange between paramagnets, due to orbital overlap, may also lead to line broadening, but under some circumstances (exchange) narrowing can result. Both dipole–dipole and exchange effects depend primarily on the distance between the paramagnets. These effects can be reduced by diluting (at the molecular level) the paramagnet in a diamagnetic host. The first 'casualties' of decreasing magnetic dilution are usually ligand hyperfine structure (because it is usually the smallest interaction), followed by the metal hyperfine structure. The individual hyperfine lines broaden, overlap, and finally produce a single broadened line.

A few selected examples which illustrate the effects of the different magnitudes of dipole–dipole and exchange interactions compared to those of the metal hyperfine and the electronic Zeeman effect are given in the following sections.

3.2.1 Electron–Electron Dipole Interactions Less than the Metal Hyperfine, but no Exchange

An example of this situation can be found[14] in the single crystal EPR spectra of $[VOCl_2(tppo)_2]$. Here the spectra are essentially those expected for a diluted vanadium(IV) centre. However, the dipole–dipole interaction makes a contribution to the peak–peak linewidth, ΔB(p–p), which supplements the inherent linewidths for the molecule. These effects are orientation dependent. When the total ΔB(p–p) and the metal hyperfine splittings are comparable in magnitude the resulting spectrum may have an

unusual appearance Instead of the expected $(2I + 1)$ lines, it may be difficult to recognize any specific number of hyperfine components Some selected examples of such spectra are in Figure 15

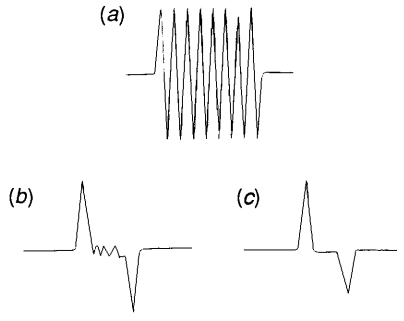

Figure 15 Spectra showing the effect of linewidth *versus* hyperfine splitting, A, for a selection of orientations in an undiluted single crystal of $[VOCl_2(triphenylphosphineoxide)_2]$ (a) $A = 19\ 33$ mT, ΔB(p-p) = 7 68 mT, (b) $A = 9\ 71$ mT, ΔB(p–p) = 9 53 mT, (c) $A = 7\ 19$ mT, ΔB(p–p) = 9 74 mT

3 2 2 *Weak Extended Exchange*

Occasionally in undiluted crystals, which apparently consist of isolated monomeric centres, we observe EPR spectra unlike those expected for a monomer, or for any discrete polymeric unit These unusual spectra are often explicable in terms of electron–electron dipole and exchange interactions which are less than or equal to the metal hyperfine coupling Here the exchange extends throughout the crystalline lattice in either one, two, or three dimensions (*i e* weak extended exchange) The first reported[15] example of such a system was the weak one-dimensional exchange system, $[N(Bu^n)_4]_2[^{63}Cu(mnt)_2]$, mnt = maleonitriledithiolate A weak two-dimensional exchanging system[16] is provided by $[H_2tmen][VO(malonato)_2(H_2O)]\ 2H_2O$, where H_2tmen = *N,N,N′,N′*-tetramethylethylenediaminium The single crystal spectra of each of these compounds are both orientation- and temperature-dependent The vanadium compound provides a particularly rich spectrum, and examples of its temperature variation when the magnetic field is parallel to the V=O direction are shown in Figure 16 Apart from the spectra in the temperature range *ca* 200 to 180K, none of these spectra have the appearance expected for an isolated monomer or for any discretre polymeric unit The methods required to interpret such spectra are beyond the scope of this review, but they are well documented [15 17]

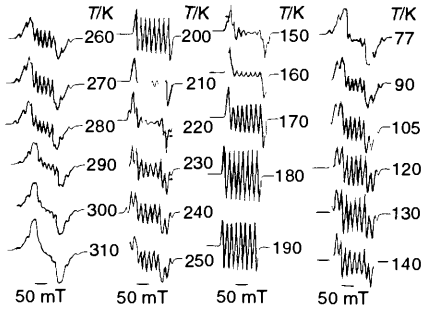

Figure 16 The temperature variation of the EPR spectrum when the applied magnetic field is parallel to the terminal VO direction in a single crystal of undiluted $[H_2tmen][VO(malonato)_2(H_2O)]\ 2H_2O$

3 2 3 *Exchange Greater than the Metal Hyperfine Splitting*

When the exchange interaction is greater than the metal hyperfine splitting, but it is less than the microwave energy ($|K(\theta)| < |J| < h\nu$), then a broad unstructured resonance may be observed The peak–peak linewidths in the spectra are, however, less than those expected for total resolution of all the hyperfine components An example of this is provided[18] by undiluted $[VO(Mequin)_2]$, where Mequin = 2-methylquinolin-8-olato In this compound a single broad line is observed at all orientations of the crystal The peak–peak linewidths range from *ca* 10 mT to 45 mT, depending upon the crystal orientation The expected spread of the spectrum for complete resolution of the metal hyperfine lines would be 38 mT to 121 mT It is possible to estimate $|J|$ from the linewidth dependence if three dimensional exchange is assumed [19] Under these conditions,

$$\Delta B(\text{p–p}) = 2M_2(\text{t})/|J| \qquad (5)$$

where ΔB(p–p) is the peak–peak separation in the first derivative spectrum, $|J|$ is the exchange interaction, and $M_2(\text{t}) = M_2(\text{d}) + M_2(\text{h})$, with $M_2(\text{h})$ equal to the second moment of the hyperfine interaction and $M_2(\text{d})$ is the second moment of the dipolar interaction $M_2(\text{d})$ can be calculated from the crystal structure data using Van Vleck's equation,[20] whilst $M_2(\text{h})$ is obtained *via* the g and A tensors from a diluted single crystal study and Slichter's general method of calculating moments [21]

For the above compound, this type of analysis gave a value of 38 mT for J

3 2 4 *Exchange Greater than the Microwave Energy*

When $|J|$ exceeds the energy of the microwave radiation the separate identities of chemically identical, but magnetically inequivalent, paramagnets at a general orientation may be lost Where two separate signals are expected in the absence of exchange there is now only one which occurs with a g value which is the arithmetic mean of the g values of the individual paramagnets at that orientation [22a] Under these conditions it is *important* to note that the principal g values are a *property of the crystal* and these will not generally correspond to the principal values for the individual paramagnets Even in a single crystal the exchange interactions destroy valuable information, since the principal g values for the individual paramagnets can only be obtained from the principal crystal g values if the direction cosines of the former are already known [22b]

When $|J| \gg h\nu$, and the exchange takes place over a very large number of centres throughout the crystal, we may observe a single sharp line when a more complicated spectrum is expected This phenomenon is known as exchange narrowing [20] The exchange causes rapid motion of an individual electron spin throughout the solid This has the effect of completely averaging metal hyperfine and electron–electron dipolar interactions, which would otherwise have a broadening effect It is sometimes possible to estimate $|J|$ from the peak–peak linewidth For a three dimensional exchange the relationship for a Lorentzian shaped line is

$$\Delta B(\text{p–p}) = 2M_2(\text{d})/\sqrt{3}|J| \qquad (6)$$

where $M_2(\text{d})$ is the second moment of the dipolar interaction

4 Ligand Hyperfine Interactions

In *d* transition metal compounds the ligand hyperfine interaction (designated by a) is usually smaller than the metal hyperfine interaction, this relative order of these interactions will be assumed throughout the present discussion Initially the use, and the limitations of CWEPR will be explored One of the major disadvantages of CWEPR is the effects of inhomogeneous line broadening, which often prevent the observation of ligand hyperfine splittings However, let us initially put aside these problems and examine some of the effects which we expect to observe Starting with any given spectrum, in the absence of ligand hyperfine interactions, we then expect additional splittings Thus each line in the basic spectrum will be split into a

number of new components depending on the types of ligand nuclei with which the unpaired electron interacts Thus a single ligand nucleus with nuclear spin I will cause a splitting into $2I + 1$ lines of equal relative intensity If the interaction of the unpaired electron is with n equivalent nuclei each with nuclear spin I, then we should observe a splitting into $\{2I_{eff}(max) + 1\}$ lines, where $I_{eff}(max) = nI$ The relative intensities of these new lines will not be equal, but will be determined by the coefficient of x^{M_I} in the following expansion

$$(x^I + x^{I-1} + x^{I-2} + \quad + x^{-I+1} + x^{-I})^n \qquad (7)$$

An example of this is shown in Figure 17 for the frozen solution spectrum of $[VO(dedtp)_2]$, where dedtp = diethyldithiophosphate There are two equivalent phosphorus atoms in this compound, which results in each of the vanadium hyperfine lines being split into a 1 2 1 triplet (^{31}P is in 100% natural abundance with $I = 1/2$)

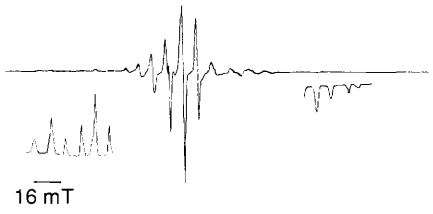

Figure 17 The X band spectrum of $[VO\{S_2P(OEt)_2\}_2]$ in toluene at 77 K

The above example is one in which the ligand hyperfine splitting is significantly greater than the linewidths of the individual resonances When the linewidths (due to inhomogeneous line broadening mechanisms) become comparable to or greater than the ligand hyperfine splittings we obtain either incomplete resolution of the ligand hyperfine splittings or fail to resolve any of the splittings An example[23] where the ligand hyperfine splitting is comparable to the linewidth is provided by the diluted crystals of $[InCl(VO)Cl_2(tmu)_2]$, where tmu = *N N N′ N′*-tetramethylurea In a powder sample of this compound no ligand hyperfine components could be resolved, see Figure 18 However, at selected orientations in a single crystal each vanadium hyperfine line showed further splittings, see Figure 19 These extra splittings can be accounted for in terms of two equivalent chloride ligands [23]

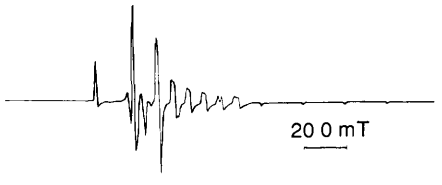

Figure 18 The Q-band powder spectrum of $[InCl\{VO\}Cl_2(tmu)_2]$, where tmu = *N N N′ N′* tetramethylurea, at 298 K ν = 34 974 GHz

This last example highlights at least one major problem associated with powder CWEPR, although improvements in resolution can sometimes be obtained by taking measurements at low microwave frequencies [24] However, if CWEPR fails to resolve ligand hyperfine splittings, when their presence is suspected, then other methods have to be tried These other methods are multiple resonance techniques such as electron nuclear double resonance (ENDOR) and pulsed techniques such as electron spin echo envelope modulation (ESEEM) Although these methods are technically more difficult than CWEPR they are less sensitive to line broadening effects, and in addition they provide a more direct measure of nuclear quadrupole and nuclear Zeeman effects These latter techniques look more directly at the energy separations (due to nuclear effects) in the individual m_S manifolds Indeed they measure the nuclear magnetic resonance (NMR) spectrum of the (highly) paramagnetic system The essential differences in the way in which the various types of spectra arise are illustrated in Figures 20 to 22, *via* simplified examples

In the CWEPR experiment the sample is continuously irradiated with a fixed microwave frequency, whilst varying the magnetic field When the condition $\Delta E = h\nu$ and the selection

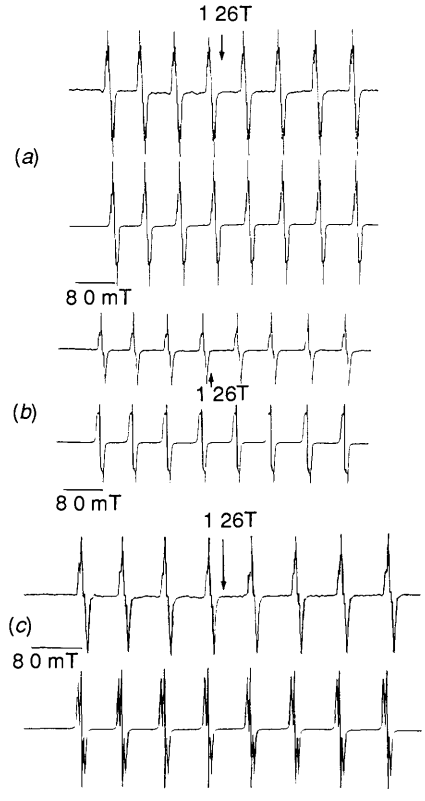

Figure 19 A comparison of the experimental (upper) and simulated (lower) spectra in the *AC* plane of a single crystal of $[InCl\{VO\}Cl_2(tmu)_2]$, where tmu = *N N N′ N′*-tetramethylurea The relative orientations were (a) 170°, (b) 150°, (c) 60°

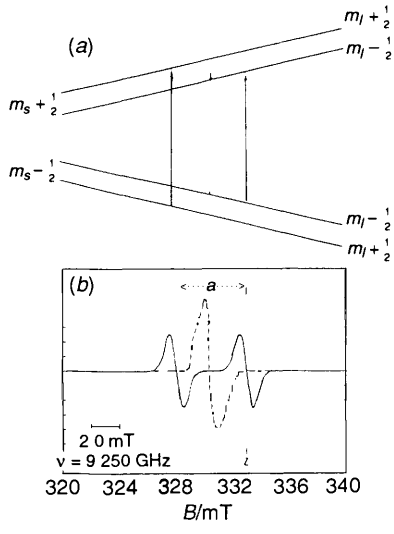

Figure 20 Diagram showing the origins of the hyperfine lines in CWEPR spectrum for a system with $S = 1/2$ and $I = 1/2$ (a) energy levels, (b) first derivative spectrum The dashed lines refer to the situation in the absence of the hyperfine interaction

rule $\Delta m_S = \pm 1$, $\Delta m_I = 0$ are both satisfied there will be an absorption of microwaves This leads to the EPR spectrum in Figure 20b

In an ENDOR experiment the magnetic field is set at the value for an EPR transition, for example the $(m_S = -1/2, m_I = 1/2) \leftrightarrow (m_S = 1/2, m_I = 1/2)$ transition in Figure 21a If the microwave power is high enough to give significant saturation of the EPR signal, and the system is swept with radiofrequency radiation, then when the radiofrequency equals the frequency for transitions between the energy levels in each m_S manifold there will be an increase in the EPR absorption When this absorption is recorded as a function of the radiofrequency the spectrum in Figure 21b will be observed In this example for $a < 2\nu_N$, where a is the hyperfine coupling constant and ν_N is the free atom resonance frequency at the magnetic field of the experiment, the two observed frequencies are [25]

$$\nu_1 = \nu_N - a/2 \quad (8)$$

$$\nu_2 = \nu_N + a/2 \quad (9)$$

In an ESEEM experiment we again set the magnetic field at a value corresponding to an EPR transition, but now the system is subjected to a sequence of intense pulses of microwave radiation The subsequent free induction decay signal, obtained as a function of the delay time between the initial pair of pulses, is modulated by the superposition of frequencies corresponding to those for transitions between the energy levels in each of the m_S manifolds [4 26] This is illustrated in Figure 22b by the simulated example of a three pulse experiment where the free induction decay has been subtracted This spectrum is in the time domain The frequencies associated with the modulations are obtained by a Fourier transform of this spectrum into the frequency domain The result of this is shown in Figure 22c

There is an approximate hierarchy of the usefulness of EPR techniques in relation to the magnitude of the hyperfine interaction CWEPR is best for measuring large interactions ($>$ *ca* 0 5mT), ENDOR is most useful in the approximate range 0 5—0 1 mT, whilst ESEEM is more suited to measuring even smaller hyperfine interactions However, the ranges over which these techniques are applicable do overlap In a system where there are several different magnitudes of hyperfine interactions, the use of all three techniques may be required in order to measure the full range of interactions An example of this is the single crystal CWEPR, ENDOR, and ESEEM studies[27] of $[TcNCl_4]^-$, diluted in the diamagnetic compound $[Ph_4As][TcOCl_4]$ Where appropriate, the hyperfine tensors, the quadrupole tensors, and the nuclear Zeeman effects on ^{99}Tc, $^{35\,37}Cl$, and $^{14\,15}N$ were measured These data allow a detailed description of the bonding in the high symmetry (C_{4v}) $[TcNCl_4]$ ion Thus the combined use of CWEPR, ENDOR, and ESEEM can give a very detailed description of the electronic structure of transition metal complexes

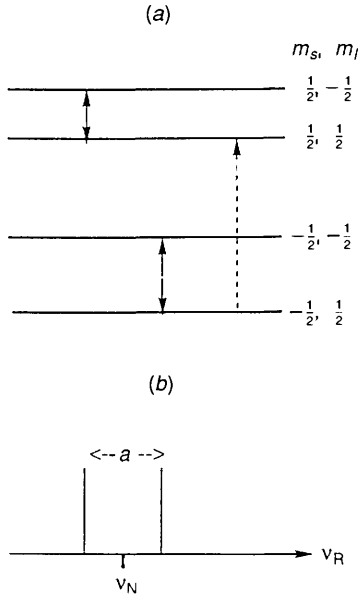

Figure 21 An illustration of the origins of ENDOR transitions in a system with $S = 1/2$ and $I = 1/2$ (a) Energy levels at a fixed magnetic field for $a < 2\nu_N$, (b) ENDOR spectrum as a function of the applied radiofrequency The dashed line represents the EPR transition which is being monitored

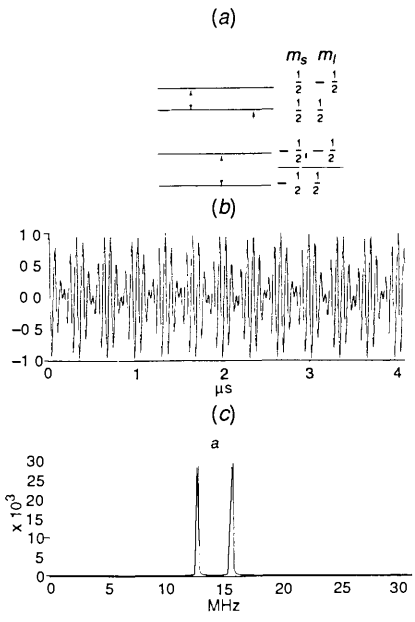

Figure 22 An illustration of the origins and the form of the ESEEM spectrum from a system with $S = 1/2$ and $I = 1/2$ (a) Energy levels at a fixed magnetic field for $a < 2\nu_N$, (b) the three-pulse spectrum in the time domain ignoring the decay, (c) the Fourier transform of the spectrum in (b) The dashed line represents the EPR transition which is being monitored

Acknowledgements The author wishes to thank Drs M S Austerberry, D Collison, J R Morton, and K J T Taylor, and Mr S S Turner for helpful discussions

4 References

1 F E Mabbs and D Collison, 'Electron Paramagnetic Resonance of *d* Transition Metal Compounds', Elsevier, Amsterdam, 1992
2 J R Pilbrow, 'Transition Ion Electron Paramagnetic Resonance Clarendon Press, Oxford, 1990
3 Ref 2, chapter 9, C P Poole, Jr and H A Farach, *Appl Spectrosc Rev*, 1983, **19**, 167, A Schweiger, *Struct Bonding (Berlin)*, 1982, **51** 1
4 Ref 2, chapter 10, A Schweiger, *Agnew Chem Int Ed Engl*, 1991 **30**, 265, L Kevan, 'Time Domain Electron Spin Resonance', ed, L Kevan and R N Schwartz, Wiley, New York, 1979, chapter 7, L Kevan, 'Modern Pulsed and Continuous Wave Electron Spin Resonance', Wiley, New York, 1990, chapter 5, A Schweiger, *ibid*, chapter 2
5 Ref 1, (a) chapters 2 and 4, (b) chapters 3 and 5
6 E M Armstrong, M S Austerberry, D Collison, S N Ertok, C D Garner, M Helliwell, and F E Mabbs, *J Chem Soc Chem Commun*, submitted for publication
7 D Collison, F E Mabbs, J H Enemark, and W E Cleland, Jr *Polyhedron*, 1986, **5**, 423, D Collison, D R Eardley, F E Mabbs K Rigby, and J H Enemark, *Polyhedron*, 1989, **8**, 1833 D Collison, F E Mabbs, and K Rigby, *Polyhedron*, 1989 **8**, 1830
8 D S Schonland, *Proc Phys Soc London*, 1959, **73**, 788, A Lund and T Vanngard, *J Chem Phys*, 1965, **42**, 2979
9 J R Morton and K F Preston, *J Magn Reson*, 1983, **52**, 457
10 D Collison, F E Mabbs, K Rigby, and W E Cleland, Jr, *J Chem Soc Faraday Trans*, 1993, accepted for publication

11 N M Atherton, 'Electron Spin Resonance, Theory and Applications', Ellis Horwood, Chichester, 1973, p 182
12 G R Luckhurst, *Mol Phys*, 1966, **10**, 543, S H Glarum and J H Marshall, *J Chem Phys*, 1967, **47**, 1374, A Hudson and G R Luckhurst, *Chem Rev*, 1969, **69**, 191
13 D Kivelson, *J Chem Phys*, 1960, **33**, 1094, R Wilson and D Kivelson, *J Chem Phys*, 1966, **44**, 154, Ref 1 p 1179 and references therein
14 B Gahan and F E Mabbs, *J Chem Soc Dalton Trans*, 1983, 1713
15 K W Plumlee, B M Hoffmann, J A Ibers, and Z G Soos, *J Chem Phys*, 1975, **63**, 1926
16 D Collison, B Gahan, and F E Mabbs, *J Chem Soc Dalton Trans*, 1983, 1705
17 B Gahan and F E Mabbs, *J Chem Soc Dalton Trans*, 1983, 1695, Ref 1, chapter 17
18 D Collison, B Gahan, and F E Mabbs, *J Chem Soc Dalton Trans*, 1987, 111
19 G F Kokoska, 'Low Dimensional Cooperative Phenomena', ed H J Keller, Plenum, New York, 1975, p 171, P M Richards, *ibid*, p 147
20 J H Van Vleck, *Phys Rev*, 1948, **74**, 1168
21 C P Slichter, 'Principles of Magnetic Resonance', Harper and Row, New York, 1963, p 50 and 3rd Edition, Springer-Verlag, Berlin, 1990, p 71
22 (*a*) D M S Bagguley and J H E Griffiths, *Proc Roy Soc (London)*, 105, **A201**, 366, (*b*) Ref 1, p 73
23 D Collison, F E Mabbs, and J Temperley, *Spectrochim Acta*, 1991, **47A**, 691
24 Ref 2, p 51
25 Ref 11, p 366
26 W B Mims, *Phys Rev B*, 1972, **5**, 2409, 1972, **6**, 3543
27 R Kirmse, K Kohler, U Abram, R Bottcher, L Golic, and E DeBoer, *Chem Phys*, 1990, **143**, 75, R Kirmse, K Kohler, R Bottcher, U Abram, M C M Gribnau, C P Keijzers, and E DeBoer, *Chem Phys*, 1990, **143**, 83